

Contents lists available at ScienceDirect

Colloids and Surfaces A: Physicochemical and Engineering Aspects

journal homepage: www.elsevier.com/locate/colsurfa



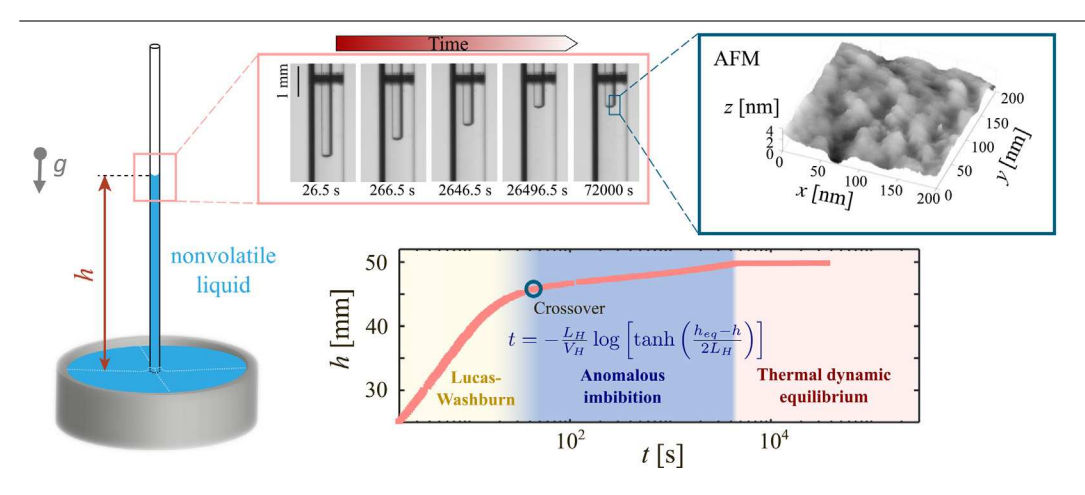


Anomalous near-equilibrium capillary imbibition induced by nanoscale surface topography

Menghua Zhao a, Aktaruzzaman Al Hossain b, Carlos E. Colosqui b,c,d,*, Matthieu Roché a

- a Matière et Systèmes Complexes, CNRS UMR 7057, Université Paris Cité, 10 Rue A. Domon et L. Duquet, 75013 Paris, France
- ^b Department of Mechanical Engineering, Stony Brook University, NY 11794, USA
- ^c Department of Applied Mathematics and Statistics, Stony Brook University, Stony Brook, NY 11794, USA
- ^d The Institute of Energy: Sustainability, Environment, and Equity, Stony Brook University, Stony Brook, NY 11794, USA

GRAPHICAL ABSTRACT



HIGHLIGHTS

- · Nanoscale topographic features induce anomalous capillary imbibition in simple tubes or pores.
- · The crossover to anomalous behavior is predicted by considering topographic parameters and the capillary diameter.
- The anomalous behavior can be prevented or promoted by modifying the tube or pore radius.

ARTICLE INFO

Keywords: Capillary driven imbibition Nanoscale surface topography Lucas–Washburn

ABSTRACT

This work reports that the nanoscale surface topography induces a crossover from the classical Lucas—Washburn imbibition dynamics to a long-lived anomalously slow regime observed near thermodynamic equilibrium conditions. A compact analytical model considering the interplay between interfacial wetting, thermal motion, and the nanoscale physical topography accounts for experimental observations for the case of capillary rise of different nonvolatile liquids in simple glass tubes. Analytical predictions supported by topographic analysis via atomic force microscopy indicate that topographic features with a specific range of nanoscale dimensions

^{*} Corresponding author at: Department of Mechanical Engineering, Stony Brook University, NY 11794, USA.

E-mail addresses: carlos.colosqui@stonybrook.edu (C.E. Colosqui), matthieu.roche@univ-paris-diderot.fr (M. Roché).

determine the crossover condition and anomalous imbibition rate. Our findings have important implications for the scientific understanding and technical application of capillary imbibition and suggest strategies to control the adsorption of specific liquids in porous materials with complex surface topography.

Glossary	
A_d	Projected defect area
ΔU	Energy perturbation magnitude
\mathcal{F}	Free energy
h	Liquid column height
h_c	Crossover height
h_{eq}	Equilibrium height
h_f	Topographic feature height
é	Energy perturbation period
ℓ_c	Capillary length
ℓ_f	Topographic feature length
$\theta_{ea}^{'}$	Equilibrium contact angle
θ_Y	Young contact angle
ξ	Damping coefficient

1. Introduction

The phenomenon of capillary driven imbibition is among the most studied in interfacial science owing to its relevance to numerous natural and industrial processes such as liquid transport in porous media [1-4], electrolyte imbibition of porous electrodes [5-7], the wetting of fabrics [8,9] and powders [10,11], additive manufacturing [12,13], and microfluidic devices for liquid handling [14-17]. The classical theoretical description of capillary imbibition relies on mechanical models involving inertia, viscous hydrodynamic friction, gravitational effects and the driving capillary force. For the case of capillary rise in simple and smooth geometries (i.e., capillary driven imbibition in smooth vertical tubes or pores), Jurin's law [18,19] predicts that mechanical equilibrium is attained when the rising liquid reaches the equilibrium height $h_{eq} = 2\gamma \cos \theta_Y / (\rho g R)$ with γ the surface tension of the liquid, θ_Y the Young contact angle, ρ the density of the liquid, g the acceleration of gravity, and R the radius of the tube. The surface of the solid is conventionally assumed as topographically smooth and chemically homogeneous, while fluid and solid phases are separated by sharp interfaces.

The general analytical treatment of capillary rise is complex even for simple geometries when considering short-time inertial effects [20–24]. However, as the column height h=h(t) increases and inertial effects become negligible, the system enters a regime described by the celebrated Lucas–Washburm (LW) equation [25,26]

$$\dot{h} = \frac{\rho g R^2}{8\mu} (h_{eq}/h - 1),\tag{1}$$

where μ is the liquid viscosity. A key assumption of this description is that the contact angle is constant and equal to the equilibrium contact angle $\theta_{eq} = \theta_Y$, as predicted by Young's law. While the validity of this assumption is not trivial, the LW equation accounts accurately for experimental observations for small imbibition rates $\dot{h} \ll \gamma/\mu$ [27–32].

Anomalous behavior with large deviations from LW predictions via Eq. (1) has been reported in porous media with complex networks of micro-scale pores [33–35]. This anomalous behavior, characterized by slow imbibition rates, has been attributed to the random non-local dynamics of the wetting front, contact line pinning, and spatial fluctuations of the capillary pressure, which are ignored in the LW

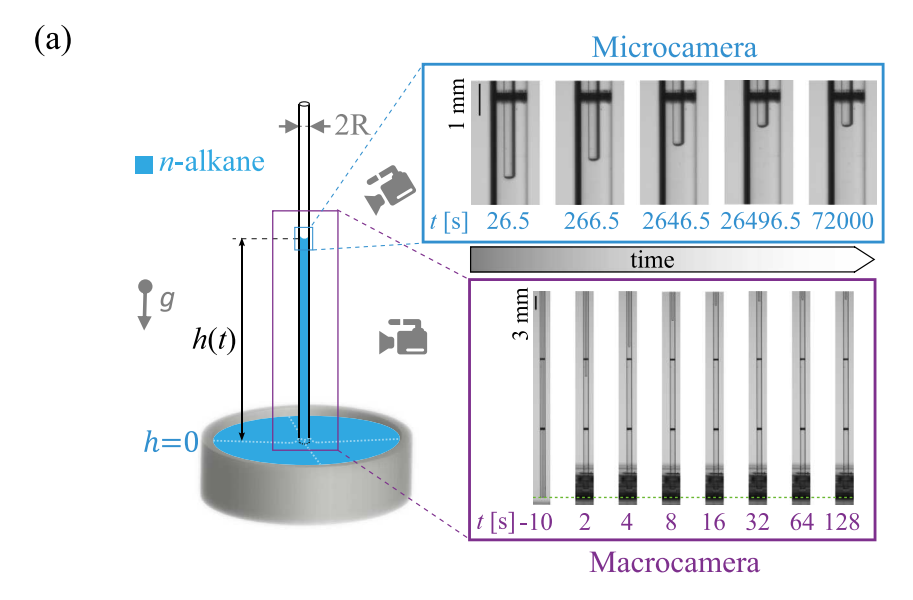
equation [33,34,36–38]. Deviations from LW predictions have been also reported and rationalized for capillaries with sharp corners of micro/macroscale dimensions [39–41]. Furthermore, various interfacial phenomena such as colloidal particle adsorption, shear-driven drainage, and droplet spreading [42–47] show an anomalously slow relaxation to equilibrium after a regime crossover from the initial non-equilibrium dynamics. Notably, these anomalous behaviors have been attributed to surface energy barriers induced by nanoscale surface topography on macroscopically smooth surfaces.

To the best of our knowledge, no prior study has characterized and rationalized the observation of anomalous capillary rise in a macroscopically smooth capillary with simple geometry due to the effects of the nanoscale surface topography. A small number of studies report that prewetting of the surface is needed to observe agreement with conventional LW predictions [27,31]. Here, we report that capillary rise experiments performed over several hours in capillary tubes display a predictable crossover from conventional LW dynamics to an anomalously slow rise near equilibrium. To rationalize this phenomenon, we propose an analytical description based on a Langevin-type equation accounting for thermal motion and energy perturbations induced by the nanoscale surface topography. The model produces close agreement with our experimental observations and the magnitude of its parameters is supported by topographic analysis of the surface of the capillaries via atomic force microscopy (AFM).

2. Experiments

We analyze the case of a liquid with constant mass density ρ , surface tension γ , viscosity μ , and temperature T that rises within a vertical capillary of radius R much smaller than the capillary length $\ell_c = \sqrt{\gamma/(\rho g)}$ (Fig. 1a). The liquids in this study are three homologous alkanes with low vapor pressures (Sigma Aldrich, purity 99%; tetradecane ($C_{14}H_{30} \ge 99\%$, $\rho = 762 \text{ kg/m}^3$, $\gamma = 26.1 \text{ mN/m}$, $\mu = 2.1$ mPa s, and $P_{vap} = 2.0$ Pa at 25 °C), pentadecane ($C_{15}H_{32} \ge 99\%$, $\rho = 769 \text{ kg/m}^3$, $\gamma = 27.1 \text{ mN/m}$, $\mu = 2.3 \text{ mPa s}$, and $P_{vap} = 0.7 \text{ Pa}$ at 25 °C), and hexadecane ($C_{16}H_{34} \ge 99\%$, $\rho = 770 \text{ kg/m}^3$, $\gamma = 27.5$ mN/m, $\mu=3.4$ mPa s, and $P_{vap}=0.2$ Pa at 25 °C)). We assume thermal and chemical equilibrium with the much less viscous ambient air. We use glass capillaries (Hirschmann ringcaps 5 µL and 20 µL) with two different inner radii, $R = 140 \,\mathrm{um}$ and $R = 310 \,\mathrm{um}$ (5% uncertainty). Capillaries are used as received, without precleaning or prewetting. Liquids are poured into a borosilicate glass petri dish (Pyrex, diameter 30 mm). A lid with a tight hole to insert the capillary tube covers the dish to prevent contamination and further minimize evaporation of the nonvolatile liquid during long exposure to the ambient. All experiments are performed at a controlled temperature $T=25\pm1$ °C. Further details on the experimental protocol and reproducibility can be found in Appendices A and B.

A "microcamera" (Imaging Source, DFK camera) records the displacement of the meniscus at the top of the liquid column with a spatial resolution of $6.0 \, \mu m/pixel$ (top right panel in Fig. 1a). We use a subpixel technique [48] to detect displacements as small as $1.2 \, \mu m$. A "macrocamera" (Andor Zyla 5.5) captures an overall view of liquid rise from the initial contact to the final equilibrium height with a resolution of $42.2 \, \mu m/pixel$ (bottom right panel in Fig. 1a). Images are processed with the software package FiJi [49] to extract the column height h(t) measured from the flat bath interface to the bottom of the rising meniscus as a function of the time t elapsed since contact. Fig. 1b shows the column height evolution h(t). At early times, the



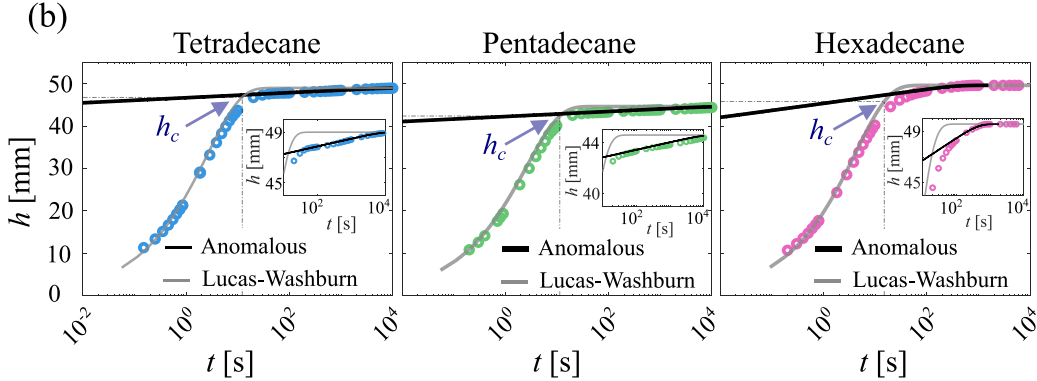


Fig. 1. Capillary driven imbibition in a vertical glass microcapillary. (a) Experimental setup. Image sequences are for pentadecane in the 140- μ m microcapillary. Top panel: microcamera view at t = 26.5, 266.5, 2646.5, 26496.5 s and 72000 s; scale bar: 1 mm. Bottom panel: macrocamera view at t = -10, 2, 4, 8, 16, 32, 64 and 128 s; scale bar: 3 mm. Dashed green line: position of the flat bath surface. (b) Column height h(t) and regime crossovers for three alkanes in the 140- μ m microcapillary. Analytical predictions (see legend) for the crossover height h_c (Eq. (4)), LW dynamics (Eq. (1)), and anomalous rise regime (Eq. (8)) employ the parameters reported in Table 1. The insets show a close- μ 0 of the near-equilibrium anomalous regime.

three alkanes show a fast increase of the column height that slows down as the system approaches equilibrium, which we defined at the height h_{eq} for which there is no detectable change for at least 6000 s. While experiments agree closely with the LW model (Eq. (1)) for typical observation times $t\lesssim 10$ s, substantial discrepancies arise for longer times. In particular, the time to reach the experimentally determined equilibrium height is over two orders of magnitude larger than that predicted by the LW equation.

3. Theory

To rationalize our experimental observations we will consider the effects of thermal fluctuations and energy perturbations induced by nanoscale surface topography. The time evolution of the liquid height h(t) is governed by a Langevin-type equation [43,44,50]

$$\xi \dot{h} = -\frac{1}{\xi} \frac{\partial \mathcal{F}}{\partial h} + \sqrt{2k_B T \xi} \eta(t), \tag{2}$$

where $\xi = 8\pi\mu h$ is the damping coefficient assuming energy dissipation is dominated by Poiseuille flow in the narrow capillary, $\eta(t)$ is a zero-mean unit-variance uncorrelated noise, and the system free energy is

$$\mathcal{F} = \frac{\rho g \pi R^2 h^2}{2} - 2\pi R \gamma \cos \theta_Y h + \frac{\Delta U}{2} \sin \left(\frac{2\pi h}{\ell} + \phi \right). \tag{3}$$

The first and second terms in Eq. (3) are, respectively, the gravitational potential energy and the interfacial free energy determined by

the Young contact angle θ_Y , which both appear in the LW equation (Eq. (1)). The third term is a single-mode energy perturbation of magnitude ΔU , period ℓ , and phase ϕ , induced by nanoscale surface topography and/or chemical heterogeneities. Since $\ell \ll h_{eq}$, we can arbitrarily adopt $\phi = -2\pi h_{eq}/\ell$ so that mechanical equilibrium is exactly attained at the height h_{eq} for which the system energy in Eq. (3) is at the global minimum, in accordance with Jurin's law.

Any finite energy perturbation of magnitude $\Delta U > 0$ in Eq. (3) produces multiple metastable states where $\partial \mathcal{F}/\partial h = 0$, sufficiently close to equilibrium, when $|h_{eq} - h| \times \rho g R^2 \ell'/2 \le \Delta U$. Hence, as $h \to h_{eq}$ the system governed by Eqs. (2)–(3) must eventually crossover from non-equilibrium dynamics driven by capillary forces to arrested dynamics dominated by metastable state transitions induced by thermal fluctuations. Such a regime crossover corresponds to the transition from conventional LW dynamics to an anomalous capillary rise and occurs around the crossover height [43]

$$h_c = h_{eq} - \alpha \frac{\Delta U}{\rho g R^2 \ell},\tag{4}$$

where a factor $\alpha = 0.5$ estimates the center of the range of heights over which the crossover takes place [43–47].

For $h\gtrsim h_c$, the column height evolution is determined by the displacement rate $\dot{h}=\mathscr{E}(\varGamma_+-\varGamma_-)$. Using Kramers theory for the (forward/backward) transition rates \varGamma_\pm gives [43]

$$\dot{h} = \frac{h_{eq}}{h} V_H \sinh\left(\frac{h_{eq} - h}{L_H}\right) \tag{5}$$

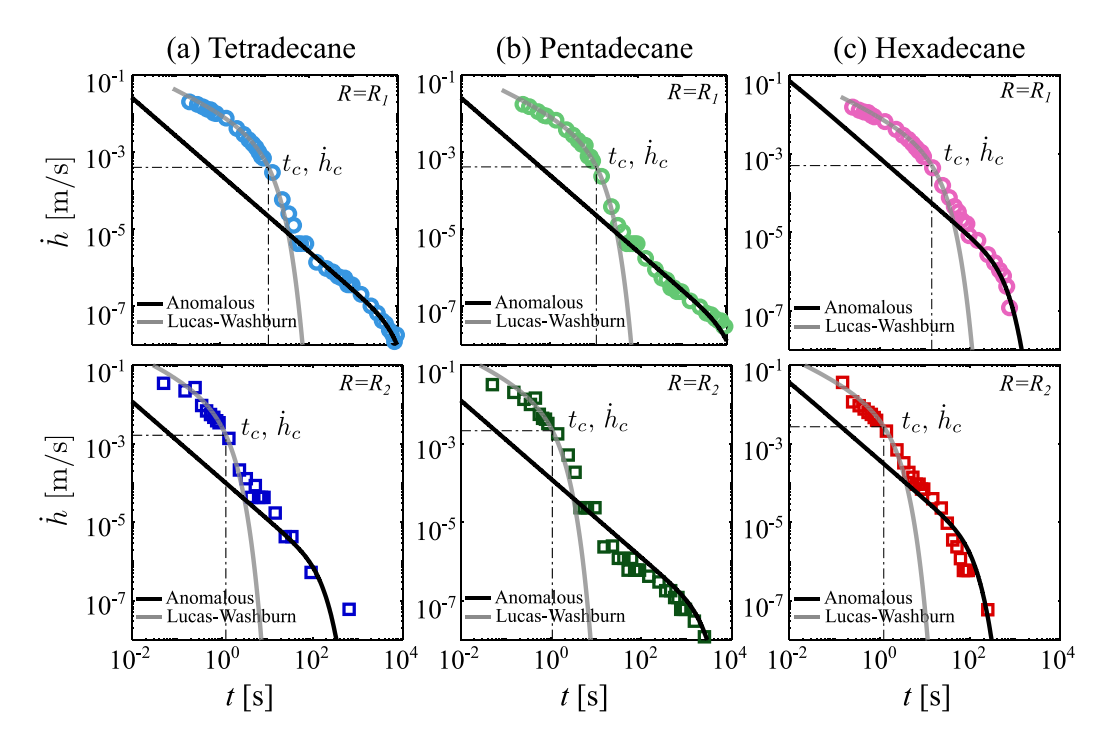


Fig. 2. Capillary rise rates $\dot{h} \equiv dh/dt$ over observation times $10^{-1} \le t \le 10^4$ s in glass microcapillaries of radius $R_1 = 140~\mu m$ and $R_2 = 310~\mu m$ for (a) tetradecane, (b) pentadecane, and (c) hexadecane. Symbols: experimental data. Grey continuous line: Eq. (1) (LW dynamics); black continuous line: Eq. (5) (anomalous regime). The crossover rate \dot{h}_c and time t_c (dot-dashed lines) are obtained by employing the crossover height h_c (Eq. (4)) in Eq. (1).

with the "hopping" length

$$L_H = \frac{2k_BT}{K\ell},\tag{6}$$

and the "hopping" velocity

$$V_{H} = \frac{\ell}{2\pi\xi_{eq}} \times \sqrt{\frac{1}{4} \left(\frac{2\pi}{\ell}\right)^{4} \Delta U^{2} - K^{2}} \exp\left(\frac{-\Delta U - \frac{1}{8}K\ell^{2}}{k_{B}T}\right), \tag{7}$$

where $K=\rho g\pi R^2$ and $\xi_{eq}=8\pi\mu h_{eq}$ is the damping coefficient prescribed by the equilibrium height. The displacement rate in Eq. (5) can be integrated to obtain the implicit relation $t=-(L_H/V_H)\times [F(x)+G(x)]+c$, where $x=(h-h_{eq})/L_H$, c is an integration constant, $F(x)=(1-xL_H/h_{eq})\times\log[\tanh(x/2)]$, and $G(x)=(L_H/h_{eq})\times[\text{Li}_2(e^{-x})-\text{Li}_2(-e^{-x})]$; here, Li₂ is the dilogarithm function. For $L_H\ll h_{eq}$, which is expected for the case of nanoscale surface features, the expression for the column height can be simplified to

$$t = -\frac{L_H}{V_H} \log \left[\tanh \left(\frac{h_{eq} - h}{2L_H} \right) \right]. \tag{8}$$

The near-equilibrium expressions for the displacement rate (Eq. (5)) and column height (Eq. (8)) derived via Kramers theory are prescribed by the energy barrier magnitude ΔU and period ℓ . Assuming that free energy perturbations in the 1D energy profile $\mathcal{F}(h)$ (Eq. (3)) are caused by nanoscale topographic features with a characteristic projected area A_d , we then define the period $\ell=A_d/(2\pi R)$ and energy barrier $\Delta U=\beta\gamma A_d$, where β is a shape factor accounting for surface energy changes associated with different 3D interfacial configurations induced by the nanoscale topography [43,44,50]. We use A_d and β as fitting parameters to account for our experimental observations of (i) the critical crossover height h_c (Eq. (4)) and (ii) the displacement rate h (Eqs. (5)–(8)) for $h>h_c$. We estimate the Young contact angle $\theta_{\gamma}\simeq\theta_{eq}$ from the measured equilibrium heights. Table 1 reports the values of the parameters employed in the model.

4. Discussion

The positive displacement rates \dot{h} reported in Fig. 2 decay monotonically over time with a marked transition from LW dynamics to the

Table 1 Parameters employed in the analytical predictions for the two microcapillaries of radius $R_1 = 140 \, \mu \text{m}$ and $R_2 = 310 \, \mu \text{m}$. The shape factor $\beta = 1 - \cos \theta_Y$ is determined using the estimate $\theta_Y = \theta_{xx}$.

Case R ₁	h _{eq} [mm]	θ_{eq} [°]	A_d [nm ²]	$\Delta U/k_BT$	ℓ [pm]	θ_c [°]
$C_{14}H_{30}$	49.0	11.3	86.75	10.67	0.099	18.2
$C_{15}H_{32}$	44.6	15.5	45.04	9.71	0.051	24.9
$C_{16}H_{34}$	49.6	17.7	21.25	6.73	0.024	28.6
Case R_2	h_{eq} [mm]	θ_{eq} [°]	A_d [nm ²]	$\Delta U/k_BT$	ℓ [pm]	θ_c [°]
$C_{14}H_{30}$	22.0	12.3	59.64	8.69	0.031	19.8
$C_{15}H_{32}$	20.9	14.0	55.72	10.11	0.029	22.5
$C_{16}H_{34}$	22.2	19.2	18.68	6.96	0.009	31.1

anomalous capillary rise regime near equilibrium. As expected, we do not observe recession of the meniscus (i.e., negative displacement rates) after reaching the equilibrium height where $h \to 0$, due to the negligible evaporation of the studied nonvolatile liquids (see Appendix C). While the LW model (Eq. (1)) describes the initial capillary rise dynamics, the proposed model (Eqs. (5)–(8)) accounts for the late near-equilibrium evolution of h by using the model parameters reported in Table 1. The same finding is reported in Fig. 1b for the column height evolution. The reported values of A_d and β (cf. Table 1) give the characteristic energy barriers $\Delta U \simeq 6.7$ to $10.7~k_BT$ and periods $\ell \sim 10^{-14}$ m. We note that ℓ in our model is determined by the average displacement of the full contact line perimeter over a single surface feature of nanoscale area A_d and therefore it is much smaller than the physical distance between localized surface features [43].

An important feature of the proposed analytical model is the prediction of the conditions for the crossover from LW dynamics to the anomalous regime. The crossover heights h_c predicted via Eq. (4) are in good agreement with the heights at which the transition is observed experimentally (i.e., 5% to 10% below h_{eq}). The use of Eq. (4) in Eq. (1) gives the corresponding critical displacement rate \dot{h}_c and time t_c reported in Fig. 2. Besides, the proposed analytical model indicates that the contact angle $\theta_c = \arccos(\rho g R h_c/(2\gamma))$ at the crossover height

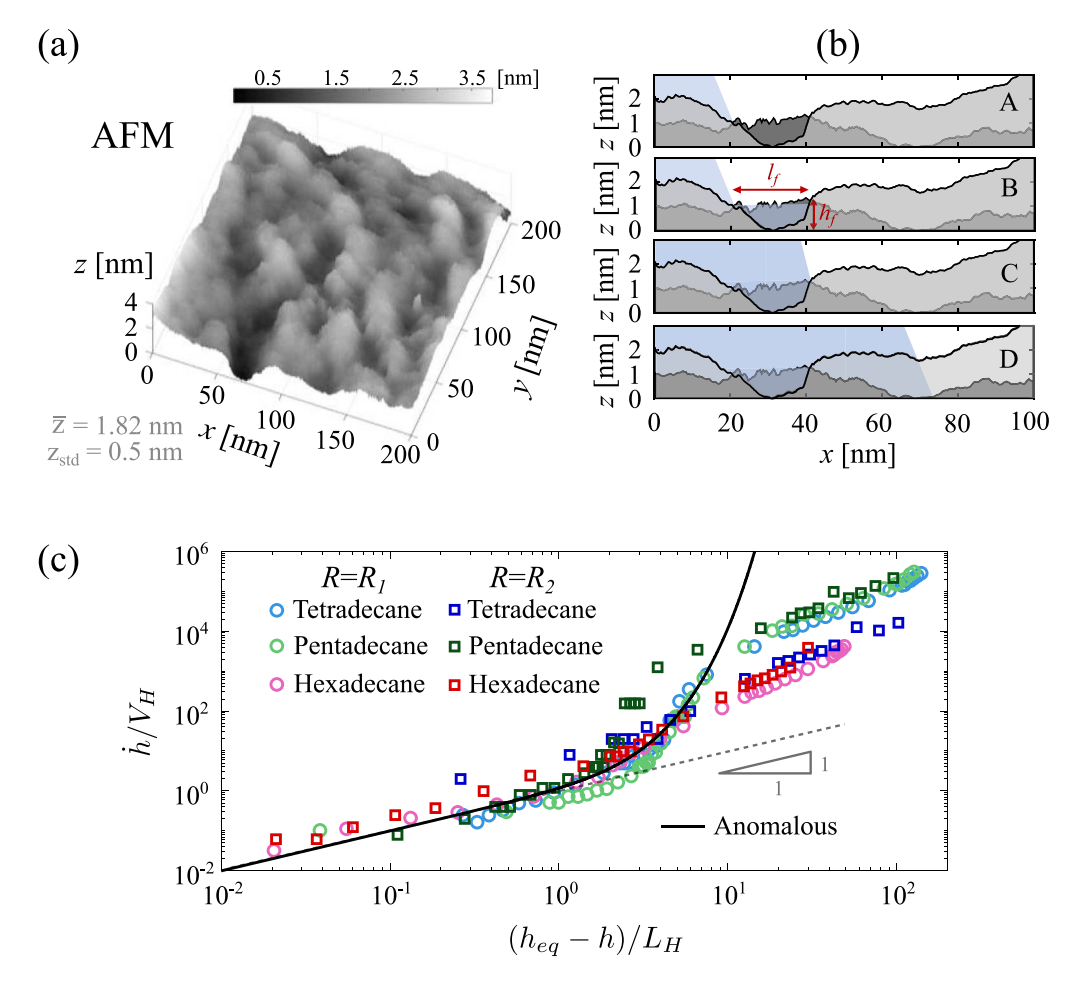


Fig. 3. Nanoscale surface topography and master curve in the stochastic regime. (a) AFM image of the surface topography height z(x, y). (b) Illustration of contact line motion over surface features with characteristic extent ℓ_f and height h_f using two overlapping AFM scans along the x-direction 10 nm apart in the y-direction. The sequence labeled (A) to (D) shows the hypothesized infiltration of critically small features via hemiwicking. (c) Dimensionless displacement rate h/V_H versus separation from equilibrium $(h_{eq} - h)/L_H$ for all tested systems. Thick black line: non-dimensionalized theoretical prediction. Grey dashed line: linear scaling in the limit $(h_{eq} - h) < L_H$.

is significantly larger than θ_{eq} (cf. Table 1), which highlights the importance of following the rising dynamics over sufficiently long times to determine equilibrium properties.

The close agreement between experiments and the proposed model relies on a set of parameters (cf. Table 1) that we assume to be induced by topographic surface features with a specific range of nanoscale dimensions. To verify this assumption we image the nanoscale topography of the inner surface of the capillaries at several different locations with an atomic force microscope (Park NX-20, k=42 N/m, $\omega_o=330$ kHz). The topographic height data z(x,y) (Fig. 3a), obtained in noncontact mode with a lateral resolution of 0.39 nm and height noise level of 0.03 nm, reports a mean topographic height $\bar{z}=1.82$ nm, standard deviation $z_{std}=0.501$ nm, and a nearly Gaussian height distribution (kurtosis $\kappa=2.96$). The AFM images (cf. Fig. 3a) show that the wetting front must move over a complex landscape of surface features with a wide range of lateral dimensions $\ell_f\sim10$ to 100 nm and a characteristic height $h_f\simeq2z_{std}\simeq1$ nm (Fig. 3a).

We now turn to the analytical estimation of the energy barriers ΔU induced by the topographic features imaged via AFM. Based on the energetics of wetting on a "rough" surface [51], hemiwicking (i.e., liquid infiltration in the local topography) is favored by features with lateral dimensions $\ell_f \leq \ell^*$ prescribed by the critical infiltration length $\ell^* = h_f \times (1/\cos^2\theta_Y - 1)^{-1/2}$. As illustrated in Fig. 3b, a local displacement of the contact line over a liquid-infiltrated feature with characteristic projected area $A_d = \pi \ell^{*2}/4$ produces a characteristic energy barrier $\Delta U = \Delta U^* = \gamma (1-\cos\theta_Y) A_d$, from which we readily determine the

shape factor $\beta=1-\cos\theta_Y$. Notably, by using $h_f=0.85$ to 1.05 nm and the experimental estimates for the equilibrium contact angle θ_{eq} we predict $\ell^*\simeq 5$ to 10 nm and the values for A_d and β reported in Table I that are employed in the analytical fits reported in Fig. 1b & Fig. 2 for the anomalous regime. It is worth noting that for surface features with lateral dimensions $\ell_f>\ell^*$ larger than the critical infiltration length, the "dry" topography (Fig. 3b) induces energy barriers given by a shape factor $\beta\simeq\sqrt{1+(h_f/\ell_f)^2-1}\sim(h_f/\ell_f)^2$ and thus we have $\Delta U\ll\Delta U^*$. Hence, the near-equilibrium displacement rate (Eq. (5)) is determined by the nanoscale features that are infiltrated by the preceding liquid film.

Based on this analysis, the characteristic "hopping" rate V_H and length L_H are prescribed by the critical surface feature length $\ell_f \simeq \ell^*$. The functional form of Eq. (5) suggests a collapse of the experimental results onto a single curve when plotting the dimensionless displacement rate h/V_H against the equilibrium separation $(h_{eq} - h)/L_H$ (see Fig. 3c). Furthermore, sufficiently close to equilibrium, $(h_{eq} - h) < L_H$, we find the linear scaling $\dot{h} = V_H \times (h_{eq} - h)/L_H$ (cf. Fig. 3c) with the characteristic displacement rate in the range $V_H \simeq 0.06$ to 4.3 μ m/s for the anomalous regime. It is worth remarking that these findings and the model in Eq. (3) are strictly valid for sufficiently large separation of scales between the characteristic dimensions of the surface topography and the radius of the capillary tube so that $\ell \ll h_{eq}$ and $h_f \ll R$. While this condition is satisfied for microcapillaries with macroscopically smooth and flat surfaces having nanoscale topographic features, the proposed model is not applicable for surface features with dimensions comparable to the capillary radius.

5. Conclusion

In summary, capillary rise experiments performed over unusually long times with non-volatile liquids under controlled ambient conditions report a crossover from LW dynamics to an anomalous regime as the column height approaches equilibrium. Compared to the classical LW equation, the characteristic defect area A_d is the only additional parameter in the model proposed to account for the experimental observations. The estimate $\theta_Y = \theta_{eq}$ for the Young contact angle results in a shape factor $\beta = 1 - \rho g R h_{eq}/(2\gamma)$ with an error linearly proportional to the uncertainty in determining h_{eq} . While the equilibrium height was determined with high accuracy owing to the extended observation times, even large relative uncertainties up to 20% in h_{eq} would result in slightly different defect areas A_d that produce the energy barrier ΔU and period ℓ reported in Table 1. We thus find that the proposed model could similarly fit the experimental data with a reasonable single estimate for the Young contact angle and small adjustments of the reported nanoscale defect areas A_d .

Our experimental and theoretical analyses thus suggest that the crossover height and the anomalous imbibition rate are determined by topographic surface features with nanometric dimensions to favor hemiwicking and infiltration of liquid preceding the contact line. Our analysis indicates that tuning the base radius-to-height ratio of nanoscale topographic features can promote or prevent the occurrence of the anomalously slow imbibition. In addition, we find that the equilibrium contact angle can be determined from the linear relation between the displacement rate and separation from equilibrium in the final stage of the anomalous capillary rise. These findings have direct implications on the design and use of capillary devices for micro/nanofluidic handling, the characterization of porous materials, and the fundamental understanding of capillary driven transport in near-equilibrium conditions.

CRediT authorship contribution statement

Menghua Zhao: Conducted the experimental work and analysis of experimental results, Manuscript writing. Aktaruzzaman Al Hossain: Performed topographic analysis via atomic force microscopy and experimental data analysis, Manuscript writing. Carlos E. Colosqui: Developed the theoretical model and validation study, Manuscript writing. Matthieu Roché: Developed the experimental study and supervised the experimental analysis, Manuscript writing.

Declaration of competing interest

The authors declare that they have no known competing financial interests or personal relationships that could have appeared to influence the work reported in this paper.

Data availability

Data will be made available on request.

Acknowledgments

C. C. acknowledges Université Paris Cité for supporting his stay at Matière et Systèmes Complexes and support for the work on theoretical model development and validation from the Center for Mesoscale Transport Properties, an Energy Frontier Research Center funded by the U.S. Department of Energy, Office of Science, Basic Energy Sciences, under award DE-SC0012673. A. A. was supported by the National Science Foundation, United States under award CBET-2016204 to perform AFM topographic analysis. M. Z. and M. R. gratefully acknowledge ANR (Agence Nationale de la Recherche), France and CGI (Commissariat à l'Investissement d'Avenir), France for their financial support of this work through Labex SEAM (Science and Engineering for Advanced Materials and Devices), ANR-10-LABX-0096 and ANR-18-IDEX-0001. This work employed resources of the Center for Functional Nanomaterials, which is a U.S. DOE Office of Science Facility, at Brookhaven National Laboratory under Contract DE-SC0012704.

Appendix A. Experimental reproducibility

Following the experimental protocol described in the main text, we performed multiple realization of the capillary rise experiments for the three studied alkanes to verify the reproducibility of the observed anomalous regime. For these experiments the capillary tubes (Hirschmann ringcaps 5 μ L and 20 μ L) were employed as received from the supplier without prewetting with the alkanes or pre-cleaning. The column height h(t) and displacement rate h measured in these experiments are reported in Fig. A.4 for the two different capillary sizes employed (iner radius $R_1 = 140~\mu m$ and $R_2 = 310~\mu m$) and show a high degree of reproducibility. For the experiments reported in Fig. A.4, the room temperature was controlled at $T = 25.5 \pm 1~\rm ^{\circ}C$ for the tetradecane and pentadecane, and $T = 22.0 \pm 1~\rm ^{\circ}C$ was the temperature for the experiments with hexadecane.

Appendix B. Cleaning protocol

To assess the effect of pre-cleaning the glass capillary, a set of capillary rise experiments were performed by employing the following cleaning protocol. The cleaning protocol consisted of injecting successively ethanol, acetone, and distilled water through the capillaries using a syringe pump at a fixed flow rate of $100~\mu\text{L/min}$. Each of the three cleaning steps was performed for 10~min. The capillary was finally dried with pressurized nitrogen. The column height h(t) observed with and without the cleaning protocol is reported in Fig. B.5 and shows no substantial differences on the observed rise dynamics and final equilibrium height.

Appendix C. Evaporation-induced recession rates

We performed experiments with nonvolatile alkane oils ($P_{vap} \leq 2$ Pa) to prevent evaporative loss of liquid during the long observation times required to attain equilibrium. Evaporation occurs at the surface of the liquid meniscus and the saturated vapor diffuses into the ambient atmosphere where we assume that the local density of the alkane vapor becomes negligible. Hence, assuming steady-state evaporation, the diffusive vapor flux can be estimated as [52]

$$J_v = -D\frac{c_{sat}}{I},\tag{C.1}$$

where D is the vapor diffusion coefficient, $c_{sat} = P_{vap}/(RT)$ is the saturation vapor concentration prescribed by the vapor pressure P_{vap} (R is the ideal gas constant and T is the temperature), and L is the distance over which the vapor concentration decays to zero in the ambient air phase. From the diffusive vapor flux J one can estimate the rate at which the meniscus should retract in the capillary due to evaporative mass loss as

$$\dot{h}_v = \frac{J_v \mathcal{M}}{\rho},\tag{C.2}$$

where ${\cal M}$ is the molar mass and ρ is the density of the liquid phase. With a characteristic diffusion coefficient $D\sim 10^{-6}~{\rm m^2/s}~[53]$ and molar mass ${\cal M}\simeq 0.2$ kg/mol for the studied alkanes, and with $L\sim 10^{-2}$ m estimated from the length of the capillary tube, we find that $|\dot{h}_v|\lesssim 10^{-11}~{\rm m\,s^{-1}}$ and thus evaporation effects are negligible in our experiments.

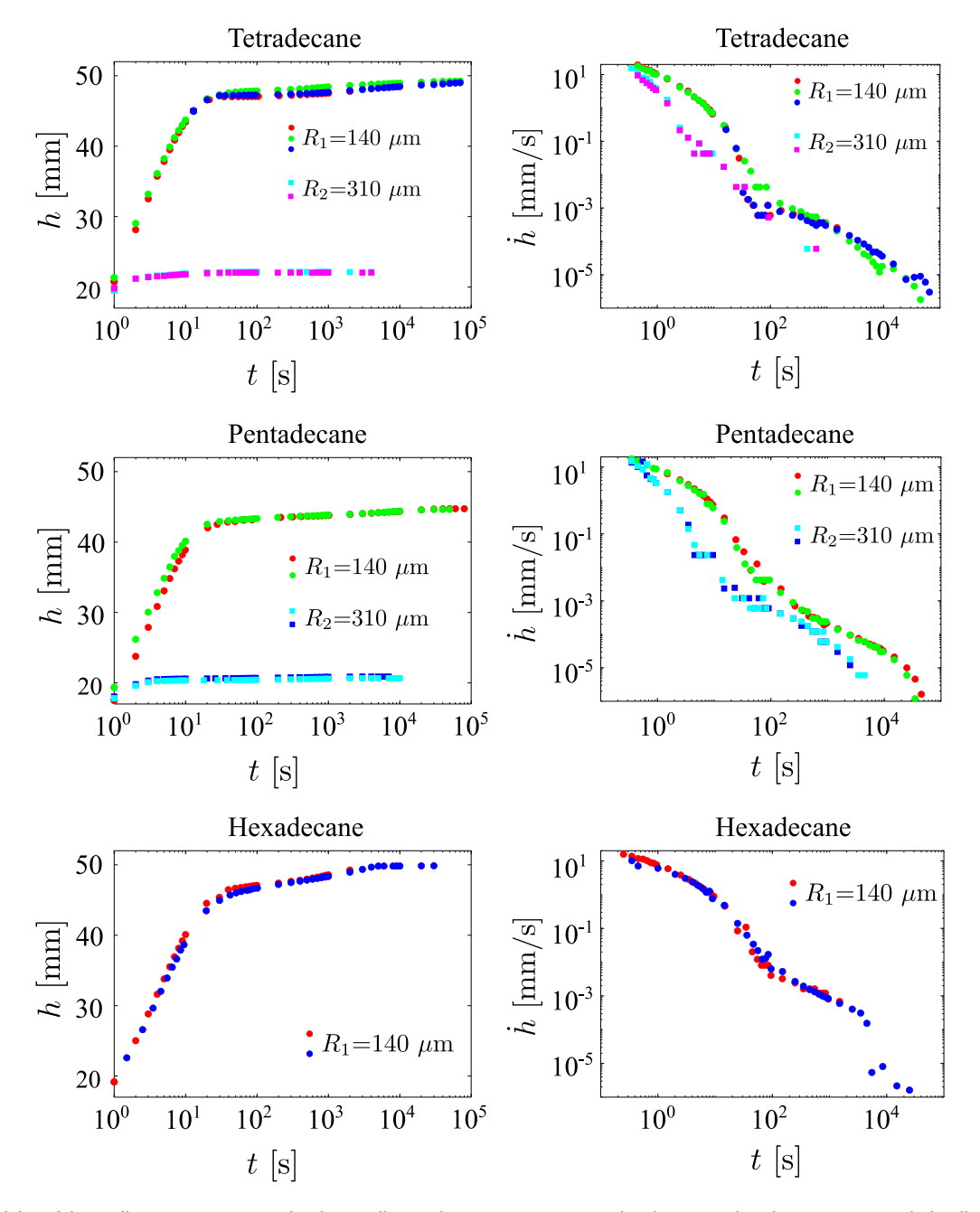


Fig. A.4. Reproducibility of the capillary rise experiments. The glass capillary in these experiments are employed as received, without prewetting with the alkanes or pre-cleaning. Different color markers (see legend) corresponds to different realizations under the same experimental conditions in a capillary of radius $R_1 = 140 \mu m$ or $R_1 = 310 \mu m$.

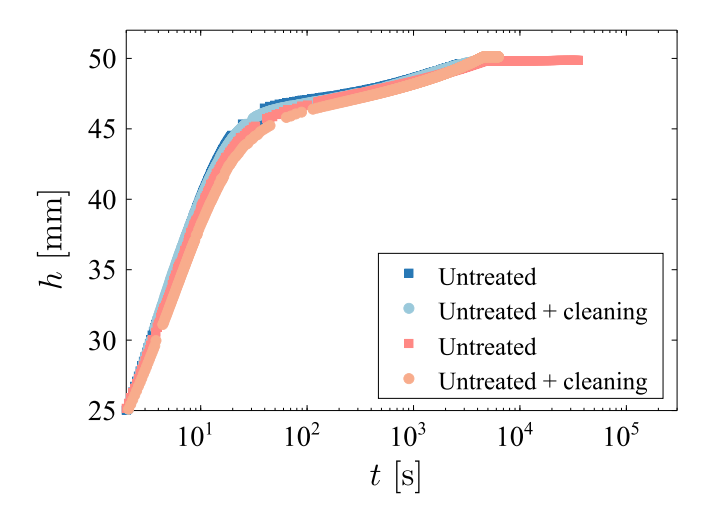


Fig. B.5. Effects of pre-cleaning. Different marker colors (see legend) correspond to different capillary rise experiments with hexadecane using a capillary untreated or pre-cleaned. The "untreated" cases correspond to capillary tubes that were not exposed to ambient air and were employed without a cleaning protocol, as received from the supplier. The "pre-cleaned" cases correspond to capillary tubes that were treated with the cleaning protocol before the experiments. The room temperature is $T=22.0\pm1~{}^{\circ}\mathrm{C}$ for all the reported cases.

References

- N.R. Morrow, Physics and thermodynamics of capillary action in porous media, Ind. Eng. Chem. 62 (6) (1970) 32–56.
- [2] N. Lu, W. Likos, Rate of capillary rise in soil, J. Geotech. Geoenviron. Eng. 130 (6) (2004) 646–650.
- [3] T. Dang-Vu, J. Hupka, Characterization of porous materials by capillary rise method, Physicochem. Probl. Miner. Process. 39 (2005) 47–65.
- [4] S. Gruener, T. Hofmann, D. Wallacher, A.V. Kityk, P. Huber, Capillary rise of water in hydrophilic nanopores, Phys. Rev. E 79 (6) (2009) 067301.
- [5] R.-S. Kühnel, S. Obeidi, M. Lübke, A. Lex-Balducci, A. Balducci, Evaluation of the wetting time of porous electrodes in electrolytic solutions containing ionic liquid, J. Appl. Electrochem. 43 (2013) 697–704.
- [6] Y. Sheng, C.R. Fell, Y.K. Son, B.M. Metz, J. Jiang, B.C. Church, Effect of calendering on electrode wettability in lithium-ion batteries, Front. Energy Res. 2 (2014) 56.
- [7] A. Davoodabadi, J. Li, Y. Liang, D. L. Wood III, T.J. Singler, C. Jin, Analysis of electrolyte imbibition through lithium-ion battery electrodes, J. Power Sources 424 (2019) 193–203.
- [8] F. Ferrero, Wettability measurements on plasma treated synthetic fabrics by capillary rise method, Polym. Test. 22 (5) (2003) 571–578.
- [9] C. Duprat, Moisture in textiles, Annu. Rev. Fluid Mech. 54 (2022) 443-467.
- [10] M. Li, G. Callegari, G. Drazer, Capillary rise in a closed column: Application to the characterization of powders, Colloids Surf. A 602 (2020) 124822.
- [11] M. Li, G. Callegari, G. Drazer, Effective capillary pressure and permeability of a granular material during imbibition in a closed column, Colloids Surf. A 648 (2022) 129280.
- [12] G. Arrabito, V. Ferrara, A. Ottaviani, F. Cavaleri, S. Cubisino, P. Cancemi, Y. Ho, B. Knudsen, M. Hede, C. Pellerito, et al., Imbibition of femtoliter-scale dna-rich aqueous droplets into porous nylon substrates by molecular printing, Langmuir 35 (52) (2019) 17156–17165.
- [13] A. Azhari, E. Marzbanrad, D. Yilman, E. Toyserkani, M.A. Pope, Binderjet powder-bed additive manufacturing (3d printing) of thick graphene-based electrodes, Carbon 119 (2017) 257–266.
- [14] C. Li, H. Dai, C. Gao, T. Wang, Z. Dong, L. Jiang, Bioinspired inner microstructured tube controlled capillary rise, Proc. Natl. Acad. Sci. 116 (26) (2019) 12704–12709.
- [15] H. Gao, Y. Liu, G. Wang, S. Li, Z. Han, L. Ren, Biomimetic metal surfaces inspired by lotus and reed leaves for manipulation of microdroplets or fluids, Appl. Surf. Sci. 519 (2020) 146052.
- [16] Z. Wang, D. Nandyala, C.E. Colosqui, T. Cubaud, D.J. Hwang, Glass surface micromachining with simultaneous nanomaterial deposition by picosecond laser for wettability control, Appl. Surf. Sci. 546 (2021) 149050.
- [17] C.E. Anderson, T. Huynh, D.J. Gasperino, L.F. Alonzo, J.L. Cantera, S.P. Harston, H.V. Hsieh, R. Marzan, S.K. McGuire, J.R. Williford, et al., Automated liquid handling robot for rapid lateral flow assay development, Anal. Bioanal. Chem. 414 (8) (2022) 2607–2618.

- [18] J. Jurin, An account of some experiments shown before the royal society; with an enquiry into the cause of the ascent and suspension of water in capillary tubes, Philos. Trans. R. Soc. Lond. 30 (355) (1718) 739–747.
- [19] M.Á. Rodríguez-Valverde, M.T. Miranda, Derivation of jurin's law revisited, Eur. J. Phys. 32 (1) (2010) 49.
- [20] D. Quéré, Inertial capillarity, Europhys. Lett. 39 (5) (1997) 533.
- [21] N. Fries, M. Dreyer, An analytic solution of capillary rise restrained by gravity, J. Colloid Interface Sci. 320 (1) (2008) 259–263.
- [22] N. Fries, M. Dreyer, The transition from inertial to viscous flow in capillary rise, J. Colloid Interface Sci. 327 (1) (2008) 125–128.
- [23] S. Das, P.R. Waghmare, S.K. Mitra, Early regimes of capillary filling, Phys. Rev. E 86 (6) (2012) 067301.
- [24] S. Das, S.K. Mitra, Different regimes in vertical capillary filling, Phys. Rev. E 87 (6) (2013) 063005.
- [25] R. Lucas, Ueber das zeitgesetz des kapillaren aufstiegs von flüssigkeiten, Kolloid-Zeitschrift 23 (1) (1918) 15–22.
- [26] E.W. Washburn, The dynamics of capillary flow, Phys. Rev. 17 (3) (1921) 273.
- [27] T.E. Mumley, C. Radke, M.C. Williams, Kinetics of liquid/liquid capillary rise: I. experimental observations, J. Colloid Interface Sci. 109 (2) (1986) 398–412.
- [28] M.N. Popescu, J. Ralston, R. Sedev, Capillary rise with velocity-dependent dynamic contact angle, Langmuir 24 (21) (2008) 12710–12716.
- [29] X. Li, X. Fan, A. Askounis, K. Wu, K. Sefiane, V. Koutsos, An experimental study on dynamic pore wettability, Chem. Eng. Sci. 104 (2013) 988–997.
- [30] M. Heshmati, M. Piri, Experimental investigation of dynamic contact angle and capillary rise in tubes with circular and noncircular cross sections, Langmuir 30 (47) (2014) 14151–14162.
- [31] P.L. Walls, G. Dequidt, J.C. Bird, Capillary displacement of viscous liquids, Langmuir 32 (13) (2016) 3186–3190.
- [32] P. Wu, A.D. Nikolov, D.T. Wasan, Capillary rise: validity of the dynamic contact angle models, Langmuir 33 (32) (2017) 7862–7872.
- [33] T. Delker, D.B. Pengra, P. z. Wong, Interface pinning and the dynamics of capillary rise in porous media, Phys. Rev. Lett. 76 (16) (1996) 2902.
- [34] M. Lago, M. Araujo, Capillary rise in porous media, J. Colloid Interface Sci. 234 (1) (2001) 35–43.
- [35] Y. Shi, M.R. Yassin, H. Dehghanpour, A modified model for spontaneous imbibition of wetting phase into fractal porous media, Colloids Surf. A 543 (2018) 64–75.
- [36] V. Ganesan, H. Brenner, Dynamics of two-phase fluid interfaces in random porous media, Phys. Rev. Lett. 81 (3) (1998) 578.
- [37] D. Geromichalos, F. Mugele, S. Herminghaus, Nonlocal dynamics of spontaneous imbibition fronts, Phys. Rev. Lett. 89 (10) (2002) 104503.
- [38] M. Alava, M. Dubé, M. Rost, Imbibition in disordered media, Adv. Phys. 53 (2) (2004) 83–175.
- [39] M.M. Weislogel, S. Lichter, Capillary flow in an interior corner, J. Fluid Mech. 373 (1998) 349–378.
- [40] A. Ponomarenko, D. Quéré, C. Clanet, A universal law for capillary rise in corners, J. Fluid Mech. 666 (2011) 146–154.
- [41] F. Gerlach, J. Hussong, I.V. Roisman, C. Tropea, Capillary rivulet rise in real-world corners, Colloids Surf. A 592 (2020) 124530.
- [42] D.M. Kaz, R. McGorty, M. Mani, M.P. Brenner, V.N. Manoharan, Physical ageing of the contact line on colloidal particles at liquid interfaces, Nat. Mater. 11 (2) (2012) 138–142.
- [43] C.E. Colosqui, J.F. Morris, J. Koplik, Colloidal adsorption at fluid interfaces: regime crossover from fast relaxation to physical aging, Phys. Rev. Lett. 111 (2) (2013) 028302.
- [44] C.E. Colosqui, J.S. Wexler, Y. Liu, H.A. Stone, Crossover from shear-driven to thermally activated drainage of liquid-infused microscale capillaries, Phys. Rev. Fluids 1 (6) (2016) 064101.
- [45] A.M. Rahmani, A. Wang, V.N. Manoharan, C.E. Colosqui, Colloidal particle adsorption at liquid interfaces: capillary driven dynamics and thermally activated kinetics. Soft Matter 12 (30) (2016) 6365–6372.
- [46] L. Keal, C.E. Colosqui, R.H. Tromp, C. Monteux, Colloidal particle adsorption at water-water interfaces with ultralow interfacial tension, Phys. Rev. Lett. 120 (20) (2018) 208003.
- [47] B.M. Jose, D. Nandyala, T. Cubaud, C.E. Colosqui, Physical ageing of spreading droplets in a viscous ambient phase, Sci. Rep. 8 (1) (2018) 1–8.
- [48] S.J. Laurence, On tracking the motion of rigid bodies through edge detection and least-squares fitting, Exp. Fluids 52 (2) (2012) 387–401.
- [49] J. Schindelin, I. Arganda-Carreras, E. Frise, V. Kaynig, M. Longair, T. Pietzsch, S. Preibisch, C. Rueden, S. Saalfeld, B. Schmid, et al., Fiji: an open-source platform for biological-image analysis, Nat. Methods 9 (7) (2012) 676–682.
- [50] C.E. Colosqui, Thermodynamics, Dynamics, and Kinetics at Liquid–Fluid and Fluid–Solid Interfaces, Elsevier, 2018.
- [51] J. Bico, U. Thiele, D. Quéré, Wetting of textured surfaces, Colloids Surf. A 206 (1–3) (2002) 41–46.
- [52] K. Beverley, J. Clint, P.I. Fletcher, Evaporation rates of pure liquids measured using a gravimetric technique, Phys. Chem. Chem. Phys. 1 (1) (1999) 149–153.
- [53] J. Kosina, J. Dewulf, I. Viden, O. Pokorska, H. Van Langenhove, Dynamic capillary diffusion system for monoterpene and sesquiterpene calibration: Quantitative measurement and determination of physical properties, Int. J. Environ. Anal. Chem. 93 (6) (2013) 637–649.